Temperature Protection System Optimization for Shaft Ventilation

Fang Han and Yuqin Zhu

School of Mechanical and Electrical Engineering, Huainan Normal University, Huainan, Anhui, China
tel:13955466649 e-mail:hanfang0554@126.com

***Abstract* — Sharp increases in gas concentration result in safety problems when poor roadway ventilation occurs as a result of frequent tripping of the shaft ventilation motor. To solve such problems, optimization of a motor temperature protection system is proposed. The system hardware architecture is optimized with ARM LPC2919 as the microprocessor and smart inverter IPM PS21865 as the power output device. The advantages of abundant ARM resources are fully considered in establishing a mathematical model for temperature protection, which realizes controlled signal dynamic tracking online and solves the problem of slow response under the traditional model. Furthermore, the use of a digital filtering algorithm improves accuracy of data processing operations. Experimental results demonstrate system stability and effectiveness after optimization.**

Keywords - system optimization; mathematical model; microprocessor; smart inverter; ventilation motor

I. INTRODUCTION

Ventilators are widely used in coal production with the rapid development of the coal industry. However, the harsh environment in a coal shaft makes the temperature protection system for a ventilator increasingly inefficient. This deficiency results in frequent trips, poor ventilation at the shaft mouth, temperature increase, and gas explosion accidents. Optimization of the temperature protection system for the ventilator is one of the important ways to guarantee the safety production of the coal mine. To enhance system controllability, the embedded microprocessor LPC2919 is used as the core, while the smart inverter PS21865 is adopted as the drive to improve the dynamic response speed of the system, Fast Fourier transform is used to establish a dynamic temperature-current tracking mathematical model. To improve the accuracy of system data acquisition, digital filtering algorithm is introduced to process the acquired signal, and system performance is tested in experiments [1] [2].

II. SYSTEM HARDWARE OPTIMIZATION

Figure 1 represents the block diagram of system hardware configuration, which mainly includes master chip ARM LPC2919, smart drives IPM PS21865, host-client, and detected circuit. The embedded microprocessor is newly developed by NXP with an ARM968E-S CPU core and one chip that integrates two TCMs with a 125 MHz operating frequency, CAN, 56 KB SRAM, and 768 KB flash memory, in addition to four 32-bit timers, two multi-channel ADCs, four 6-way PWM unit, and numerous interfaces (I/O). The embedded microprocessor LPC2919 simplifies the system hardware configuration, shortens development period, and meets the needs of the AC motor control. The LPC2919 has a computing speed of up to 80 MHz. Thus, the device meets the requirements of fast Fourier transform (FFT) and digital filtering algorithm. The temperature range of the device falls between –40 and +85 °C, thereby making it suitable for the harsh environment in the shaft. IPM PS21865 is an integrated smart inverter module that is newly developed by Mitsubishi Corporation and integrates a power switch, an IGBT drive, an over-current under-voltage protection, and other protection circuits. These features simplify the peripheral circuit design and improve system output stability. Smart sensor DSl8820 is adopted as a temperature sensing element; it achieves detection signal linearization and improves accuracy of data acquisition. RS485 networking is adopted to ensure communication between the host and client, thereby enabling real-time monitoring of motor operating conditions [3] [4] [5] [6].

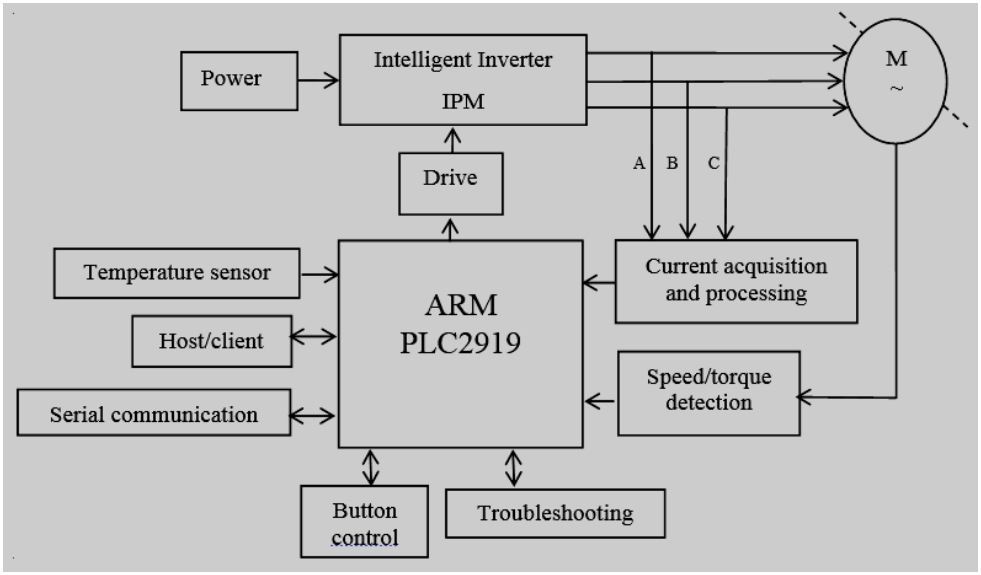

Fig. 1 Block diagram of system hardware configuration.

To ensure a high control signal input IPM, a reverser 74HC14D (as shown in Fig. 2) is added between ARM LPC2919 and IPM PS21865. This position allows the conversion of a 6-way pulse signal from the PWM module integrated inside ARM LPC2919 into a 5 V high-level voltage output, which meets IPM PS21865 input signal requirements [7].

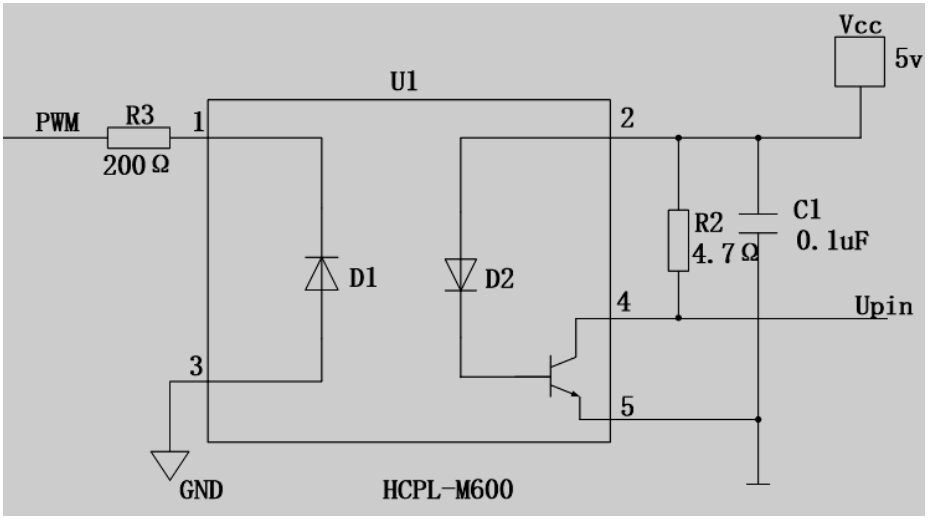

Fig. 2 IPM drive circuit.

III. SYSTEM SOFTWARE OPTIMIZATION

Major factors that influence the operational stability of a ventilator include temperature and current. Thus, the system software optimization starts from temperature and current.

A. establishment of temperature model

Temperature change and time have a nonlinear relationship. Thus, describing the relationship between the temperature θ and time t by using a specific function formula during continuous operation of the ventilator is impossible. However, the entire operation process of the motor can be split into small intervals T. The measured temperature of each of the interval T is tested online using temperature sensor DSl8820 and then sent to the A/D interface of the embedded microprocessor LPC2919, with the analog signal converted into a digital signal. The temperature-time relationship [8] can be obtained by FFT

after the digital filtering process (see Fig. 3).

$$\theta_i = (kI_{eqi}^2 - \vartheta_{i-1})(1 - e^{-t/T}), (i = 0,1,2....n) \quad (1)$$

In Formula (1), θ_i represents the temperature at the i[th] time point, θ_{i-1} represents the temperature at the i-1[th] time point, and k represents the coefficient. In view of the serious signal interference in coal mine shafts, θ_i needs to consider de-noising and using data fusion technology[9][10]. The de-noising algorithm is as follows:

First, to meet the relevant requirements of the temperature, Equation θ is required.

$$\theta = H\theta_i + R \quad (2)$$

In Formula (2), H represents the coefficient matrix for the temperature equation θ_i, and R represents the error vector.

Under the unanimity rule, the temperature values calculated by Formula (2) after extremum removal are divided into two groups, which are expressed by θ_{1k} and θ_{2k}, and $k \le \frac{1}{2}(i-1)$, respectively.

The arithmetic mean values and de-noising standard errors of the groups are expressed as follows:

$$\left.\begin{aligned} \bar{\theta}_1 &= \frac{1}{k}\sum_{k=0}^{\frac{1}{2}(i-1)} \theta_{1k} \\ \bar{\theta}_2 &= \frac{1}{k}\sum_{k=0}^{\frac{1}{2}(i-1)} \theta_{2k} \\ T_1 &= \sqrt{\frac{\sum_{k=0}^{\frac{1}{2}(i-1)} (\theta_{1k} - \bar{\theta}_1)^2}{k-1}} \\ T_2 &= \sqrt{\frac{\sum_{k=0}^{\frac{1}{2}(i-1)} (\theta_{2k} - \bar{\theta}_2)^2}{k-1}} \end{aligned}\right\} \quad (3)$$

The standard error expression of temperature fusion is obtained under the principle of batch estimation as follows:

$$\Delta T = \frac{T_1^2 T_2^2}{T_1^2 + T_2^2} \quad (4)$$

The synthetic function of dynamic temperature response is finally summarized

$$\left.\begin{aligned} T &= \left[\bar{\theta}_1\ \bar{\theta}_2\right] = \left(\Delta T \delta^{-1}\right)\theta + \Delta T H^T R^{-1} \\ &= \frac{T_2^2\,\bar{\theta}_1}{T_1^2 + T_2^2} + \frac{T_1^2\,\bar{\theta}_2}{T_1^2 + T_2^2} \\ &= \frac{1}{T_1^2 + T_2^2}(T_1^2\,\bar{\theta}_2 + \bar{T}_2^2\,\bar{\theta}_1) \end{aligned}\right\} \quad (5)$$

In Formula (5), $H = [1\,1]^T, R = \begin{bmatrix} T_1^2 & 0 \\ 0 & T_2^2 \end{bmatrix}, \delta = [T_1 T_2]^T$

Only when the calculated temperature by Formula (5) $T \le T_m$ will the ventilator work normally (assuming that T_m is the limit temperature for the motor during normal operation). When $T > T_m$, adopting software programming for protection is required.

B. establishment of the current model

Motor coil heating will cause the ambient temperature to elevate and cause a gas explosion. To control the motor current, the control relationship between Current I and Voltage U (or load torque T) needs to be deduced. Describing the relationship between Current I and Voltage U is impossible during the entire operation of the ventilator because of nonlinear temperature changes. The relationship between current and voltage [11] [12] [13] can only be deduced indirectly (e.g., using the FFT algorithm). The deduction process is as follows: Assume that the current-sampling frequency is fs, the signal source frequency is f ($f_S > 2f$), and the number of sampling points is N (assumed that N is the integral power of 2). The current sensor sampling signal is sent to the A/D interface for the embedded microprocessor LPC2919. Digital filtering is conducted with the analog signal converted into the digital signal. Finally, in accordance with pre-programmed procedures, the complex number of N point can be obtained by FFT, and every complex number point corresponds to a frequency. The current magnitude response relationship can be obtained by modulo operation, and the mathematical model for the real and imaginary parts of the fundamental wave of different phase of current can be deduced by FFT. Next, with the A-phase current taken as an example, the real part can be expressed as

$$I_{ka} = \frac{2}{N}\sum_{k=0}^{n-1} I_{Ka-1} \cos(2k\pi / N) \quad (6)$$

De-noising is necessary to eliminate signal interference. The standard error formula for the real part

In Formula (6), I_k represents the current at the k[th] time point, and I_{ka-1} represents the current at the k-1[th] time point.

after de-noising as above is

$$\Delta I_k = \frac{\sum_{k=0}^{\frac{1}{2}(k-1)} (I_{1i} - I_1)^2 \sum_{k=0}^{\frac{1}{2}(k-1)} (I_{2i} - I_2)^2}{\sum_{k=0}^{\frac{1}{2}(k-1)} (I_{1i} - I_1)^2 + \sum_{k=0}^{\frac{1}{2}(k-1)} (I_{2i} - I_2)^2} \quad (7)$$

In Formula (7), I_{1i}, I_{2i} represents the current of Group I_{ka}, and, I_1, I_2 represents arithmetic mean values of different groups. When Formulas (6) and (7) are combined, the mathematical model for dynamic tracking of the A-phase current is obtained as follows:

$$I_{ka} = \frac{2}{N}\sum_{k=0}^{n-1} I_{Ka-1}\cos(2k\pi / N) + \frac{\sum_{k=0}^{\frac{1}{2}(k-1)} (I_{1i} - I_1)^2 \sum_{k=0}^{\frac{1}{2}(k-1)} (I_{2i} - I_2)^2}{\sum_{k=0}^{\frac{1}{2}(k-1)} (I_{1i} - I_1)^2 + \sum_{k=0}^{\frac{1}{2}(k-1)} (I_{2i} - I_2)^2} \quad (8)$$

When the current calculated by Formula (8) $I_{ka} \leq I_m$, (assume I_m is the rated current during normal operation of the motor), the ventilator works stably. When $I_{ka} > I_m$, software programming needs to be adopted for protection. The methods for B/C-phase are similar; thus, they will not be repeated here.

C. applications of digital filtering algorithm in ventilator control

Given the harsh environment in shafts, significant data acquisition errors could exist and thus result in motor runaway. Thus, acquired data need to undergo digital filtering [14] to ensure operational accuracy of the embedded microprocessor LPC2919, as presented in the flowchart in Fig. 3.

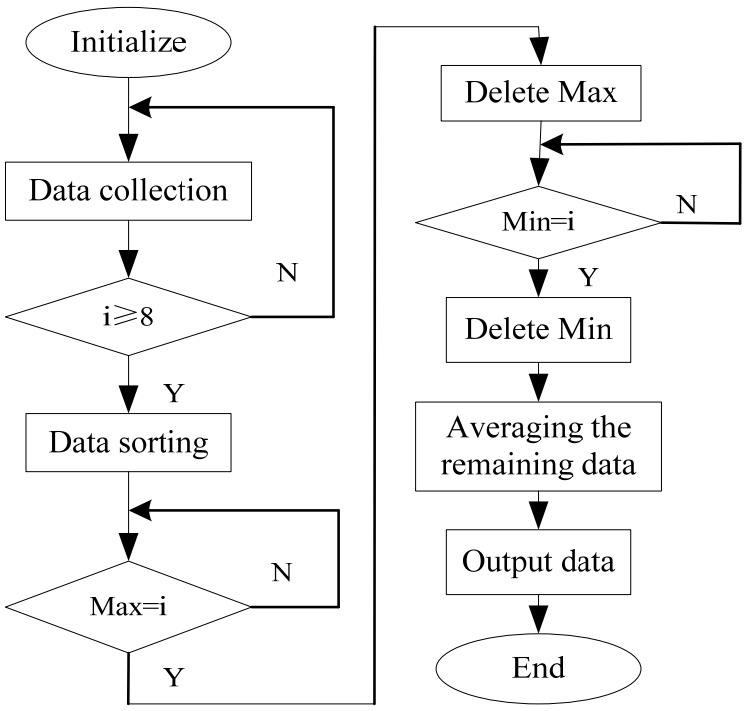

Fig. 3 Flowchart of digital filtering algorithm

IV. EXPERIMENTAL VERIFICATION

Figure 4 shows the ARM LPC2919-based experimental control system model, which mainly includes an ARM master control module, driver module, and communication module, among others, with the schematic diagram basically remaining the same as in Fig. 1.

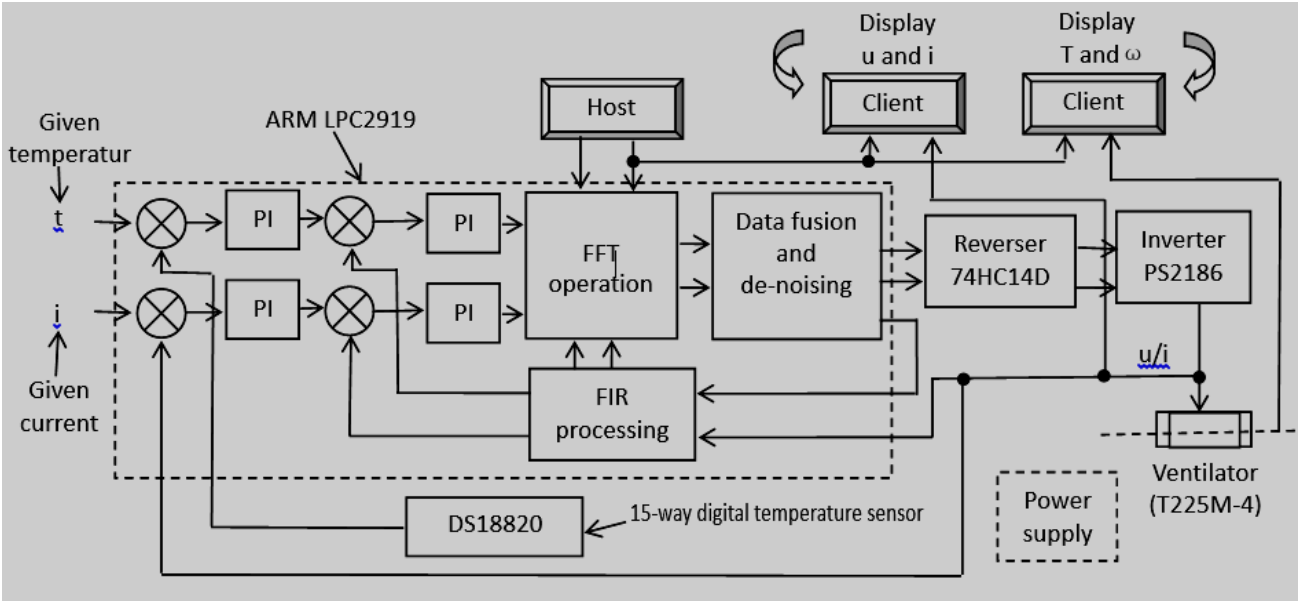

Fig. 4 Experimental control system model

The main experimental equipment includes a ventilator (Model No.W9-19-12.5) and a drive motor (Y280M-4); the motor is connected in the shape of a triangle [15]. The ventilator parameters are given in Table I.

TABLE I. MAIN PARAMETERS OF THE VENTILATOR

Parameter	Meaning	Value	Unit
P_N	Rated power	90	kW
U_N	Rated voltage	380/660	V
n_N	Rated speed	1450	r/min
f_N	Rated frequency	50	Hz
K	Temperature sampling	15	/
T_N	point	1e-6	S
T	Current sampling cycle	1e-4	S
Pa	SPWM cycle	4961–4598	Pa
υ	Total head	15381–2171	m^3/h
	Flow rate	4	

To increase comparability, an experiment was first performed on the system before optimization; the obtained experimental results are shown in Fig. 5. Then, a simulation test was conducted on the system after optimization; results are presented in Fig. 6.

Speed test: When t=0 s, the motor is started at the given speed ω=900 r/min. When the ventilator runs stably, the speed increases to ω=1200 r/min. When t=0.012 s, the speed drops to ω=600 r/min.

Torque test: When t=0.006 s, the motor load suddenly increases to T=30 N.m. When the motor runs stably, the load suddenly drops to T=10 N.m at the time point of t=0.012 s.

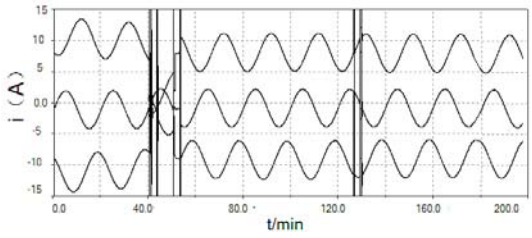

(a) Three-phase current waveform

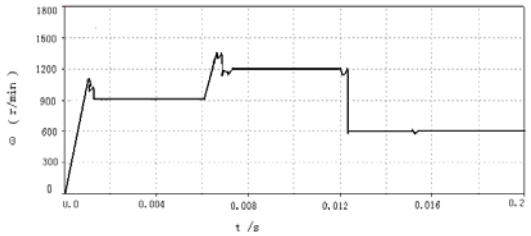

(b) Speed waveform

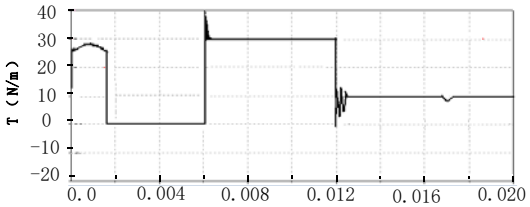

(c) Torque waveform

Fig. 5 Operating conditions of the fan system before optimization

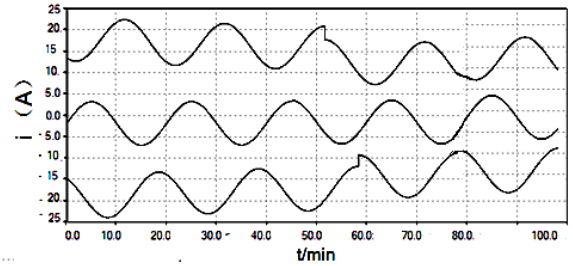

(a) Three-phase current waveform

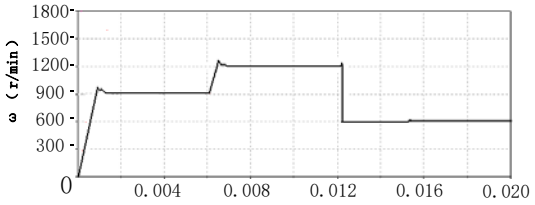

(b) Speed waveform

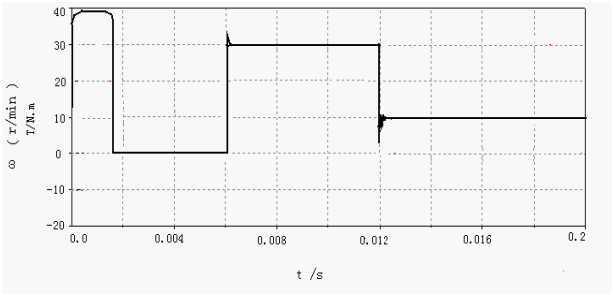

(c) Torque waveform

Fig. 6 Operating conditions after fan system optimization

Analysis of experimental results: As Fig. 5(a) shows, the system output current waveform is relatively stable, which basically solves the problem of motor tripping. However, in Fig. 6(a), the motor trips at time points of 41, 51, 127, and 129 min, thereby indicating that the system before optimization is unstable. Considering response speed, the overshoot in Fig. 5(c) is approximately 4.5%, while that in Fig. 6(c) is approximately 2.0%. The overshoot is significantly reduced, and the fluctuation is smaller. Considering the torque response, when the motor starts without load, both overshoots in the two figures reach the rated torque before 0.002 s, and then the torque quickly

returns to zero. When t=0.006 s, the motor is loaded T=30 N.m, followed by a rise of the torque to 30 N.m. When t=0.012 s, the motor load is reduced to T=10 N.m, followed by an immediate drop of 10 N.m in the torque. Clearly, the motor in either of the two control modes could work normally at the given load. However, the system torque pulsation before optimization is relatively obvious, with the torque fluctuation range at approximately ±0.06%, while the system torque fluctuation range after optimization is ±0.02% or so. The stability of system operation after optimization is thus determined.

V. CONCLUSION

The LPC2919 temperature protection optimization system based on an embedded microprocessor is characterized by a simple hardware configuration, high intelligence, short design cycle, and fast dynamic temperature-current response. The features of the system are supported by the experimental results. The optimization system is effective, feasible, and suitable for all asynchronous AC motors, especially for shafts, wells, and other places with harsh environments that require a high safety factor.

ACKNOWLEDGMENTS

The authors would like to thank the Natural Science Funding Organization of Anhui Provincial Department of Education (KJ2014A239) for financial support. At the same time, the authors would also thank Natural Science Funded Project of Huainan Normal University (2013xj58 and 2014xj49) for sponsor.

REFERENCES

[1] Y. FAN and Y. HE, Study on field-oriented induction's control system of speed adaptive estimation, Electrical Transmission 36(9), 6–8,2006.
[2] D. Li, AC speed control system. Beijing: Publishing House of electronics industry, 2010.
[3] A. Makouf, D. Diallo, H. Benbouzid et al., A practical scheme for induction mot or speed sensorless field-oriented Control, Energy Conversion IEEE Transactions 19(1), 230–231,2009.
[4] Y. BAN, X. WEI and H. JING, Design of the main fan of ARM9-based adaptive control system of the main mine, Modern Electronic Technology 8(6) 129–130,2011.
[5] H. LI, L. LU and H. CHEN, Design of control system based on ARM for electric bicycles, Electrical and Mechanical Engineering 29(9), 1069–1072,2012.
[6] Z. MA, Q. LI and Y. XU, Theory and application of the ARM cortex-core TI microcontroller. Beijing: Beijing University of Aeronautics and Astronautics Press, 2011.
[7] Y. WANG and Y. XU, A design study of dual-stator permanent magnet brushless DC motor, TELKOMNIKA (Telecommunication Computing Electronics and Control) 11(4)653–660,2013.
[8] J. LI and X. CHENG, On-line identification of the induction motor stator resistance, Motor and Control Journal 11(6), 620–624,2007.
[9] S. LI, Theory and application of the intelligent optimization algorithm. Harbin: Harbin Institute of Technology Press,2012.
[10] F.-R. ZHANG and T.-S. ZHAI, A research of control system on speed vector without sensor-less, Control System 22(1), 53–55,2006.
[11] H. XU, H. WANG, J. Tan et al., A system research on vector control based on the new model of flux -observation, System of Electric Drive 38(5), 11–14,2008.
[12] W. JIANG, A vector control system on AC induction motor based on internal model current, Mechanical and Electrical Engineering 24(4), 78–81,2007.
[13] R. LI and L. JIN, Design of frequency control system of arm-based storage battery motor vehicle SVPWM, Machines and Control Application 2(10), 34–38,2012.
[14] F. LIN and X. DU, MATLAB simulation of power electronic applications, Beijing: China Electric Power Press, 2009.
[15] Y.-Q. ZHU and G. XU, Control system of speed vector on mineral ventilation motor, Journal of Computational Methods in Sciences and Engineering 15,277–286,2015.